CrossMark

In Situ Nanomechanical Testing of Crystalline Nanowires in Electron Microscopes

YONG ZHU[1,2]

1.—Department of Mechanical and Aerospace Engineering, North Carolina State University, Raleigh, NC 27695, USA. 2.—e-mail: yong_zhu@ncsu.edu

This article reviews in situ mechanical testing of crystalline nanowires in scanning and transmission electron microscopes, focusing on bottom–up synthesized, single-crystalline nanowires. Major experimental methods including resonance, bending, tension and buckling are summarized. In addition to commonly encountered experimental issues, deformation mechanisms learned from the in situ nanomechanical characterization are discussed highlighting the roles of free surfaces, internal planar defects and point defects.

INTRODUCTION

Crystalline nanowires (NWs) are among the most important building blocks for a broad range of applications including nanoelectronics, optoelectronics, energy harvesting and storage, ultrasensitive sensing, and nanoelectromechanical devices.[1–3] These NWs generally exhibit ultrahigh mechanical strength, which makes them ideal candidates for studying fundamental deformation mechanisms at the nanoscale.[4–7] It is known that electronic band gaps change with elastic strain, so do phononic band gaps, thermal transport and other physical and chemical properties. Therefore, the ultrahigh strength also offers unprecedented opportunities to tune the functional properties of crystalline NWs through the elastic strain engineering.[5] As an example, Si NWs were found to exhibit an enormous range of elastic strain (over 12% for diameters less than 20 nm),[8] which shows promise for elastic strain engineering (e.g., the electron–hole recombination rate was found to increase sixfold at 5% strain).[9]

Crystalline NWs exhibit marked differences in mechanical behavior from their bulk counterparts as a result of large surface-to-volume ratio. Free surfaces can affect the mechanical properties of NWs in several ways. The first effect is through surface stress. Due to the small sizes of NWs, the surface stress may induce a significant compressive stress in the interior of the NWs, leading to a size-dependent yield strength.[10] The second effect leads to size effect in elasticity due to several mechanisms such as surface elasticity, bulk nonlinear elasticity (as a result of the surface stress), and surface

reconstruction.[6,11,12] In the case of metal NWs, surface dislocation nucleation becomes dominant, which differs from collective dislocation dynamics inside the microscale or bulk counterparts.[13–15]

This paper summarizes the recent advances in the field of in situ nanomechanics of bottom–up synthesized crystalline NWs in scanning and transmission electron microscopes (SEM/TEM). The paper starts with the commonly used in situ experimental methods including resonance, bending, buckling and tension. In addition to two challenges associated with these testing methods, insights learned from the in situ mechanical testing are presented highlighting the roles of free surfaces, internal planar defects and point defects.

EXPERIMENTAL METHODS AND REPRESENTATIVE RESULTS

A number of experimental methods have been developed for mechanical characterization of crystalline NWs, which can be categorized into vibration/resonance in SEM or TEM,[16–19] bending using atomic force microscopy (AFM),[20–23] and tension/bending/buckling in SEM/TEM using a nanomanipulator.[24–29] In this paper, the resonance, bending, tension and buckling methods in SEM or TEM will be discussed one by one (as shown Fig. 1), with representative results for each method. In general, the dependences of the measured Young's modulus on the equivalent NW diameter for these methods are given in Table I. It can be seen that the resonance and tension methods are less sensitive to the measurement error in NW diameter than the bending and buckling methods.
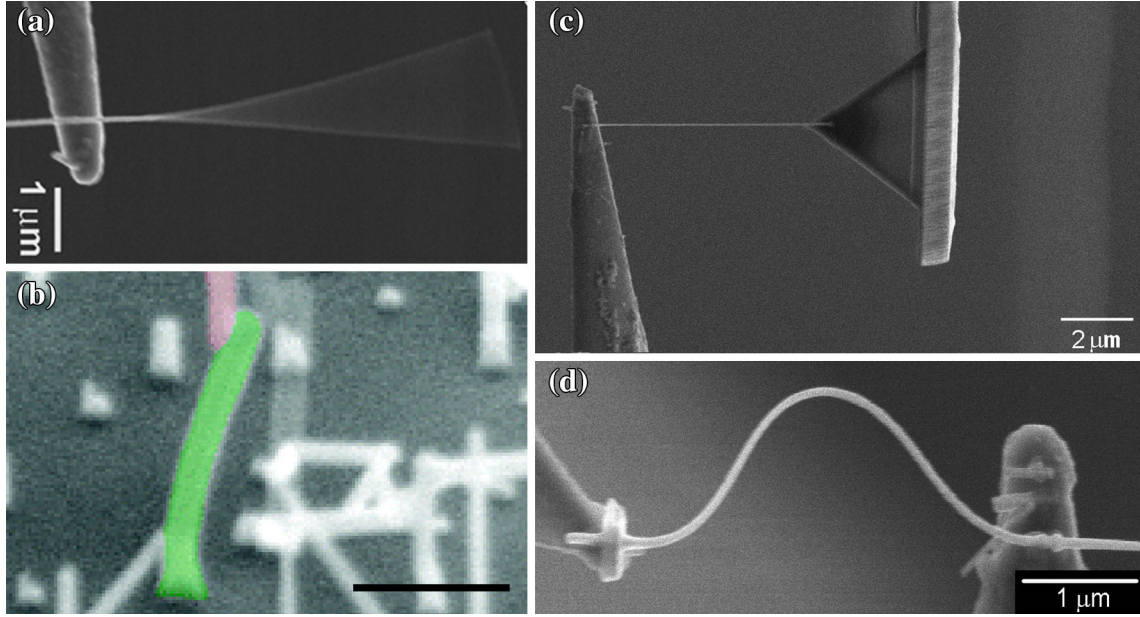
Fig. 1. (a) Resonance test. A NW is clamped on a nanomanipulator probe and excited to resonance by mechanical vibration.[18] Reprinted with permission from Ref. 18. (b) Bending test. A vertically grown NW (in green) is bent by a nanomanipulator probe (in pink).[45] Scale bar 1 μm. Reprinted with permission from Ref. 45. (c) Tension test. A NW is pulled between a nanomanipulator probe (actuator) and an AFM cantilever (load sensor).[25] (d) Buckling test. A NW is compressed to buckling between a nanomanipulator probe (actuator) and an AFM cantilever (load sensor)[25] (Color figure online).

Table I. Dependence of measured Young's modulus (E) on equivalent NW diameter (d)

	Resonance	Bending	Tension	Buckling
E	d^{-2}	d^{-4}	d^{-2}	d^{-4}

Tensile testing platforms based on microelectromechanical systems (MEMS) will be briefly discussed.[30–33] While this paper focuses on the bottom–up synthesized NWs,[34–41] some of the experimental methods presented can be used for top–down fabricated NWs and other one-dimensional nanostructures such as nanotubes.

Resonance

Resonance is a simple and widely used method to measure Young's modulus of carbon nanotubes and NWs (Fig. 1a). According to a simple beam theory, the nth mode resonance frequency of a cantilevered beam is

$$\omega_n = \frac{\beta_n^2}{L^2}\sqrt{\frac{EI}{\rho A}} \qquad (1)$$

where E is the Young's modulus, I is the moment of inertia, L is the beam length, A is the cross-sectional area and ρ is the beam density. The β_n term is the eigenvalue from the characteristic equation.[42] When the resonance frequency is measured, the Young's modulus can be calculated according to Eq. 1.

The resonance can be excited by thermal,[17] electrical[16,19] or mechanical[18] means. It is critical to distinguish so-called forced resonance and parametric resonance. Parametric resonance is a resonance phenomenon that arises because some parameter of the system is varying periodically in time.[43] Assuming the fundamental natural frequency ω_0, forced resonance occurs at driving frequency $\omega = \omega_0$, while parametric instability occurs at $\omega = 2\omega_0/n$ (n integer larger than or equal to 1). Chen et al. found that, if the NW is aligned with the nanomanipulator tip resulting in an axially applied force, parametric excitation dominates; if the force is applied transverse to the NW length, forced excitation dominates.[19] Failing to properly distinguish between these two types of resonances could lead to incorrectly measured natural frequency, which may be $2/n$ ($n = 1, 2, 3, 4$ can be observed readily in experiments) times the true natural frequency, leading to a large deviation of the Young's modulus.

When the diameters of the ZnO NWs were smaller than about 120 nm, pronounced size effect in elasticity was observed—the Young's modulus increased dramatically with the decreasing diameter.[19] When the diameters were larger than 120 nm, the Young's modulus approached that of bulk ZnO. According to the proposed core–shell composite NW model, the origin of the size dependence was attributed to the surface stiffening effect as a result of significant bond length contractions near free surfaces (which extend several layers deep into the bulk and fade off slowly).[44]

Bending

For vertically aligned NWs that are epitaxially grown on top of a substrate, bending has been used to measure the fracture strength (Fig. 1b).[45] In the bending experiment, an AFM cantilever attached to a nanomanipulator system was used to deflect a NW in the lateral direction. The applied force can be obtained from the measured deflection of the AFM cantilever. Using this method, the bending strength of [111]-oriented Si NWs synthesized by the vapor–liquid–solid (VLS) method was measured. The average strength was around 12 GP, close to the theoretical fracture strength, which indicates the high quality of the VLS-synthesized Si NWs.

In the bending experiment, a rigid nanomanipulator tip can also be used. In this case, the bending force cannot be directly measured, but the NW bending deformation and bending strain can still be measured. Chen and Zhu measured the fracture strain of ZnO NWs of a large range of diameters (85–542 nm).[46] Large strains up to 4–7% were measured before the elastic fracture. As a result of the large fracture strain and the small NW diameter, these NWs exhibited unprecedented flexibility.

Tension

Among all the mechanical testing methods, tensile testing is the most straightforward one, which can measure a full spectrum of mechanical properties such as elasticity, plasticity and fracture.[47] In situ TEM tensile testing of top–down nanostructures (e.g., using focused ion beam) have been studied.[48–50] However, tensile testing of bottom–up synthesized NWs is quite challenging due to requirements of manipulating and fixing the nanostructure and high-resolution measurement of force and displacement. Ruoff and co-workers reported the first tensile testing of individual carbon nanotubes inside SEM.[24] An individual nanotube was picked up by a sharp tip on a stiff AFM cantilever and clamped onto the tip by electron beam-induced deposition (EBID) of hydrocarbon available in the SEM chamber. The other end of the nanotube was clamped onto the tip of a compliant AFM cantilever. The stiff and compliant AFM cantilevers were used as the actuator and the load sensor, respectively, for the tensile testing.

Using fine probes (typically sharpened by electropolishing) attached to a nanomanipulator, individual nanostructures can be manipulated and harvested with minimal to no handling damage. Such a probe is stiff and can be used as the actuator for mechanical testing. Zhu et al. used a tungsten probe attached to a nanomanipulator (Klocke Nanotechnik) and a compliant AFM cantilever (as the load sensor) to conduct tensile testing of Si NWs (Fig. 1c).[8] The force resolution was 5.25 ± 0.38 nN. For NWs with diameters ranging from 15 nm to 60 nm, the stress resolution ranged from 29.7 MPa to 1.8 MPa. The strain resolution was about 0.03%. Using digital image correlation (DIC), subpixel resolution can be obtained, leading to a strain resolution of 0.01%.[51] Using this method, the Young's moduli and fracture strengths of VLS-synthesized Si NWs with diameters between 15 nm and 60 nm were measured. The Young's modulus decreased while the fracture strength increased up to 12.2 GPa, as the NW diameter decreased. The fracture strength also increased with the decrease of the side surface area; the increase rate for these Si NWs was found to be much higher than that for the microfabricated Si thin films. Repeated loading and unloading during tensile tests demonstrated that the NWs are linear elastic until fracture without appreciable plasticity, in contrast to the superplasticity observed during in situ TEM tensile testing.[52]

A microfabricated flexure beam and a nanomechanical transducer (Hysitron) have also been used as the load sensor. The measured noise floors of the force measurement for the flexure beam and the nanomechanical transducer in the SEM/FIB chamber are approximately 50 nN and 700 nN, respectively. Using such load sensors and a nanomanipulator probe, tensile tests of Cu nanowhiskers were performed.[29] Note that nanowhiskers are typically referred to a specific type of NWs that are synthesized by physical vapor deposition and contain no or negligible internal planar defects. The Cu nanowhiskers exhibited ultrahigh strengths (close to the theoretical strength) and the absence of large amounts of plasticity, which are both attributed to the small sizes and high crystalline quality of these nanowhiskers. A piezoresistive AFM cantilever has also been used as the load sensor.[53]

It is worth mentioning MEMS-based mechanical testing platforms. MEMS consist of micrometer-scale components but offer nanometer displacement and nano-Newton force resolutions. MEMS have played an important role in mechanical testing of microscale thin films.[54–56] They are showing tremendous potential to impact the nanomechanical characterization through controlled actuation with high spatial and temporal resolutions, high-resolution force/displacement measurements, integrated multi-functions and tiny size for in situ SEM/TEM testing. Zhu and Espinosa developed the first integrated nanoscale testing system using MEMS technology.[57–60] In the past decade, there has been extensive interest in developing fully-integrated MEMS-based platform for in situ SEM/TEM experimental nanomechanics.[61–64] For more details on MEMS-based nanomechanical testing, please refer to a recent review.[32]

Buckling

In situ SEM/TEM compression on micro/nanopillars have been extensively studied.[65–67] Due to the large slenderness ratio (i.e., length vs.

diameter), however, NWs typically buckle under compression. Buckling tests have been used to measure Young's moduli of several NWs such as Si,[68] ZnO[18] and Boron.[28] Similar to the tension test, the testing apparatus also includes an actuator and a load sensor, but the load sensor is typically much more compliant compared to the tensile test.

Xu et al. measured the buckling behavior of ZnO NWs using a compliant AFM cantilever as the load sensor.[25] After the NW was clamped between the nanomanipulator probe and the AFM cantilever, the NW was continuously pushed until buckling. The post-buckling shape of the NW can be clearly seen (Fig. 1d). The force and compression data were directly obtained from the SEM images, similar to the tension test. The force resolution was 0.07 ± 0.01 nN. According to the Euler buckling, the Young's modulus of the NW was calculated.

Due to the surface effect, the Young's modulus of a NW measured under different loading modes (i.e., tension and bending) can be different. For NWs under bending (including buckling and resonance), the surfaces carry the largest stress and strain; by contrast, NWs subjected to uniaxial tension undergo uniform stress across the cross-section. The Young's modulus of ZnO NWs measured from both tension and buckling tests showed the stiffening trend, i.e., it increases with decreasing diameter. In addition, a loading-mode-dependent size effect was reported; more specifically, the Young's modulus under bending was larger than that under tension for the same NW size.[25]

EXPERIMENTAL ISSUES

Effect of Clamping on Measured Mechanical Properties

In mechanical testing of nanostructures, it is common to clamp them using EBID of hydrocarbon or platinum. The clamping is not infinitely rigid as often assumed; hence, it is of relevance to investigate the effect of the clamping on the measured mechanical properties. Using the resonance test, the effect of clamping on the measured Young's modulus of NWs was investigated via a combined experimental and simulation approach, with ZnO NWs used as an example.[18] The resonance tests were performed in situ inside a SEM and the NWs were cantilevered on a tungsten probe by EBID of hydrocarbon. EBID was repeated several times to deposit more hydrocarbons at the same location. The resonance frequency increased with the increasing clamp size until approaching that under the "fixed" boundary condition. The critical clamp size was identified as a function of NW diameter and NW Young's modulus. This work illustrated the importance of considering the effect of clamping in measurements of Young's modulus using the resonance method.

Gianola and co-workers have reported that the stiffness of the EBID clamps commonly used for nanoscale tensile testing is approximately of the
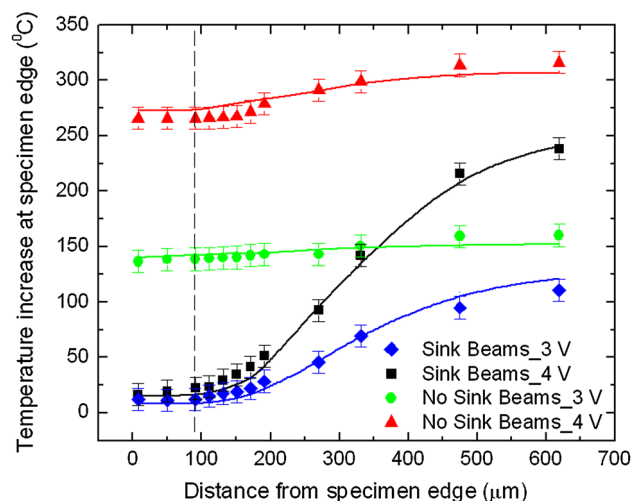

Fig. 2. Raman measurement and FEA of the temperature profile of a thermal actuator along the shuttle (starting from the specimen edge) under two different actuation voltages. Solid lines represent the FEA results and dots represent Raman measurements. The dashed vertical line shows the position of the nearest pair of heat sink beams (from the specimen edge).[70] Reprinted with permission from Ref. 70.

order of that of inorganic NW specimens.[69] As a result, inconsistent and significant errors could be introduced in measurements of displacement and hence strain and Young's modulus, depending on the stiffness of the sample and the geometry of the clamp. In addition, permanent clamp deformation could be misinterpreted as plastic deformation in the NWs. The authors suggested that a local measurement of strain be necessary for mechanical testing when EBID clamps are used. EBID deposited markers on the NW can be used for the local measurement.

Temperature Control in Thermal Actuators

MEMS thermal actuators can provide stable, displacement-controlled loading and have become widely used in nanomechanical testing.[30] However, a potential drawback of the thermal actuator is the undesired sample heating. To circumvent this problem, Zhu et al. introduced so-called heat-sink beams as a simple solution.[59] The heat-sink beams connect to the specimen end of the thermal actuator, providing heat dissipation pathways to the substrate. Recently, Qin and Zhu reported experimental measurement and multiphysics modeling of the temperature profile of the thermal actuator.[70] The temperature measurement was based on Raman scattering in air. Fully 3D multiphysics (coupled electrical–thermal–mechanical) simulation was used to treat both the air and vacuum conditions; the air and vacuum conditions are of relevance to the Raman measurement and the in situ electron microscopy testing of nanostructures, respectively. For the same thermal actuator, the Raman measurement and multiphysics modeling were carried out with and without the heat sink beams (as shown

in Fig. 2); the heat sink beams were carved out by FIB. This work clearly demonstrated that the heat sink beams play a critical role in reducing the temperature at the specimen end of the thermal actuator. To reach reasonably large actuator displacement while maintaining low temperature, several design guidelines were provided including more inclined thermal beams, more heat sink beams, small inclination angle, and relatively short heat sink beams.

INSIGHTS GAINED FROM IN SITU MECHANICAL TESTING

In situ SEM/TEM mechanical testing has helped further our understanding of how crystalline NWs deform, yield and fracture, especially when combined with atomistic simulations. Free surface, often considered as one type of planar defects, is known to have significant impact on mechanical properties of crystalline NWs including metals, semiconductors and ceramics.[4–7] In the case of metal NWs, surface dislocation nucleation has been recognized as the dominant deformation mechanism. Internal planar defects (e.g., stacking faults and twin boundaries, TBs) and point defects (e.g., vacancies, dopant and catalyst atoms) are commonly present in many VLS-synthesized semiconductor NWs[71–73] and solution-synthesized metal NWs.[74,75] It is of interest to study how dislocations nucleated from the free surfaces interact with internal planar defects and its effect on mechanical properties of NWs. Here, the scope is limited to single-crystalline NWs, thus another type of internal planar defects, grain boundary, is not discussed. Recently, a growing body of evidence suggests that nucleation of a first dislocation in a pristine crystal is associated with diffusion of point defects.[38,76–79] Below, a few representative works highlighting the effects of the three types of defects in NWs are discussed.

Effect of Free Surfaces

Surface plays the dominant role in the size effect on elasticity of NWs.[80–83] Due to a competition of factors such as bond saturation and redistribution of electron density, surfaces can be either elastically stiffer or softer than the underlying bulk material.[11,84] In addition, surface stresses, which also arise from the coordination number reduction of surface atoms, cause deformation of not only the surfaces but also the underlying bulk material to maintain the overall equilibrium,[12] which changes the elastic properties of the NW bulk (so-called bulk nonlinear elasticity). The surface stresses can cause surface reconstruction that further changes the surface elasticity and surface stress.[84,85]

Figure 3 summarizes the reported Young's moduli of Si[8,52,86–91] and ZnO[19,25,85,92–94] NWs as functions of the NW diameter. Overall, the available data are limited and scattered, which highlights the need for accurate measurements of force, displacement and cross-sectional area, as well as known boundary conditions. In spite of the data scatter, Zhu et al. showed a clear size effect for Si NWs[8]—the Young's modulus decreases with the decreasing NW diameter when the diameter is below about 30 nm (Fig. 3a), which was attributed to the surface elasticity. The trend agrees well with the DFT calculations[89] and the multiscale resonance calculations.[95] For ZnO NWs, a more consistent size effect can be seen (Fig. 3b)—the Young's modulus along the [0001] orientation increases with the decreasing NW diameter. The size effect was also attributed to the surface elasticity.[19,25,85] Xu et al. showed that the size-dependence measured in bending modes is more pronounced than the one measured under uniaxial loading, confirming the importance of the surface elasticity.[25] Size effect on the Young's modulus of metal NWs has also been reported with a stiffening trend in general—the Young's modulus increases
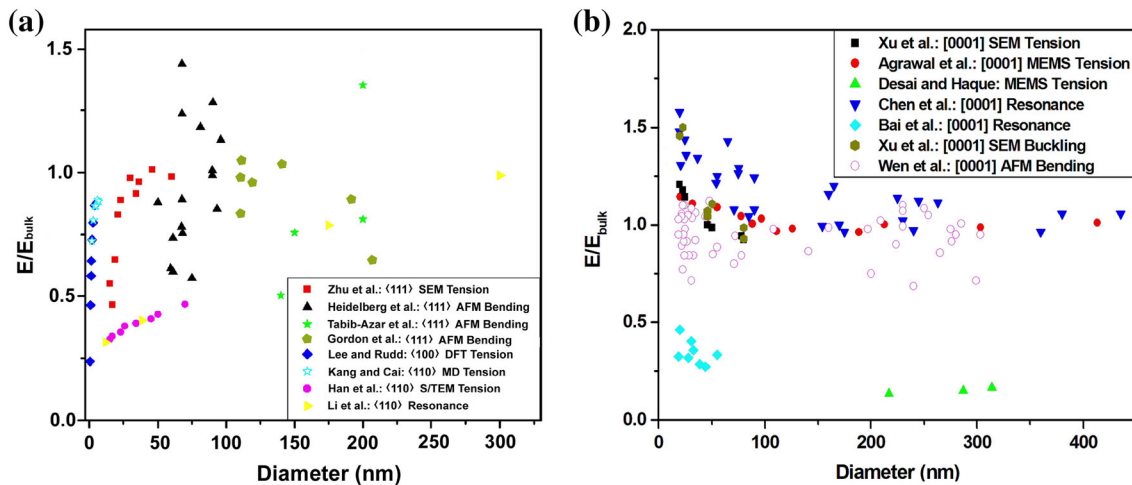

Fig. 3. (a) Summary of the size effect on the Young's modulus of Si NWs.[8,52,86–91] The data are normalized by the bulk value in the ⟨111⟩ orientation. (b) Summary of the size effect on the Young's modulus of ZnO NWs.[19,25,85,92–94] The data are normalized by the bulk value in the [0001] orientation.
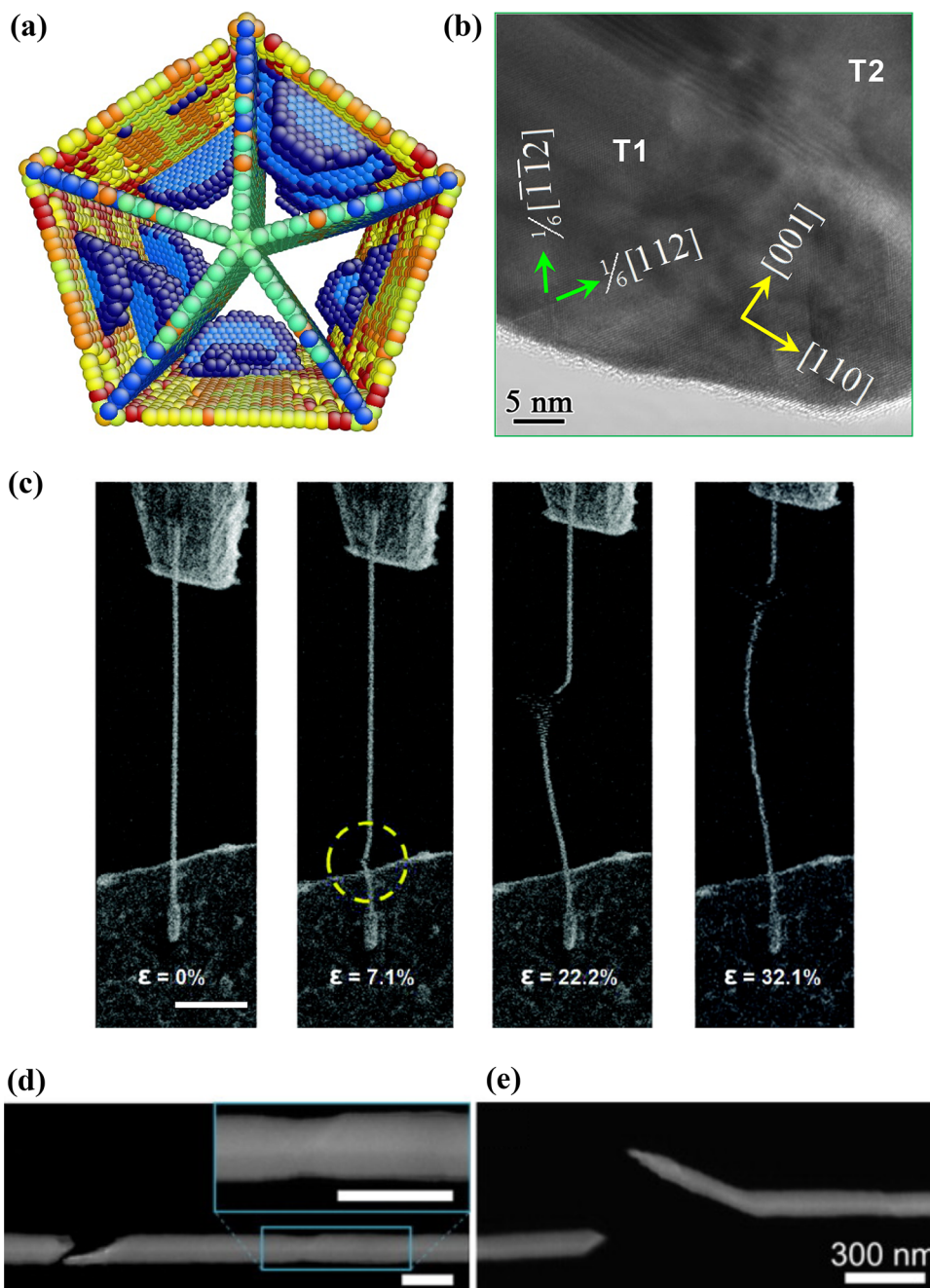
Fig. 4. (a) MD simulation (cross-sectional view) and (b) TEM image of a penta-twinned ⟨110⟩ Ag NW showing the dislocation nucleation in two equivalent slip systems.[103] Reprinted with permission from Ref. 103. (c) Snapshots of the tensile deformation of a single-crystalline ⟨110⟩ Au NW showing the coherent twin propagation.[102] *Scale bar* 1 μm. Reprinted with permission from Ref. 102. (d, e) Two modes of deformation twinning in single-crystalline ⟨110⟩ Au nanowhiskers: (d) formation of many small slip steps on multiple slip systems and (e) an extended thinned region that tilts away from the tensile direction after fracture.[101] Reprinted with permission from Ref. 101.

with the decreasing NW diameter, which has been attributed to either the surface elasticity or the bulk nonlinear elasticity.[26,81,96,97]

Slip and twinning are two major plastic deformation mechanisms for bulk metals. For metal NWs, it is not surprising that both slip (via perfect dislocations or partial dislocations)[13–15,38,98,99] and twinning[100–102] have been observed following nucleation of leading partial dislocations from free surfaces. The

competition between these deformation mechanisms is influenced by loading type, NW diameter, NW orientation, side surface orientation, and temperature, which can be reasonably explained by Schmid factors of the leading and trailing partial dislocations and generalized stacking fault energies.[7]

The slip by partial dislocations has been reported in penta-twinned Ag NWs (with five TBs perpendicular to the NW cross-section).[103] MD simulations
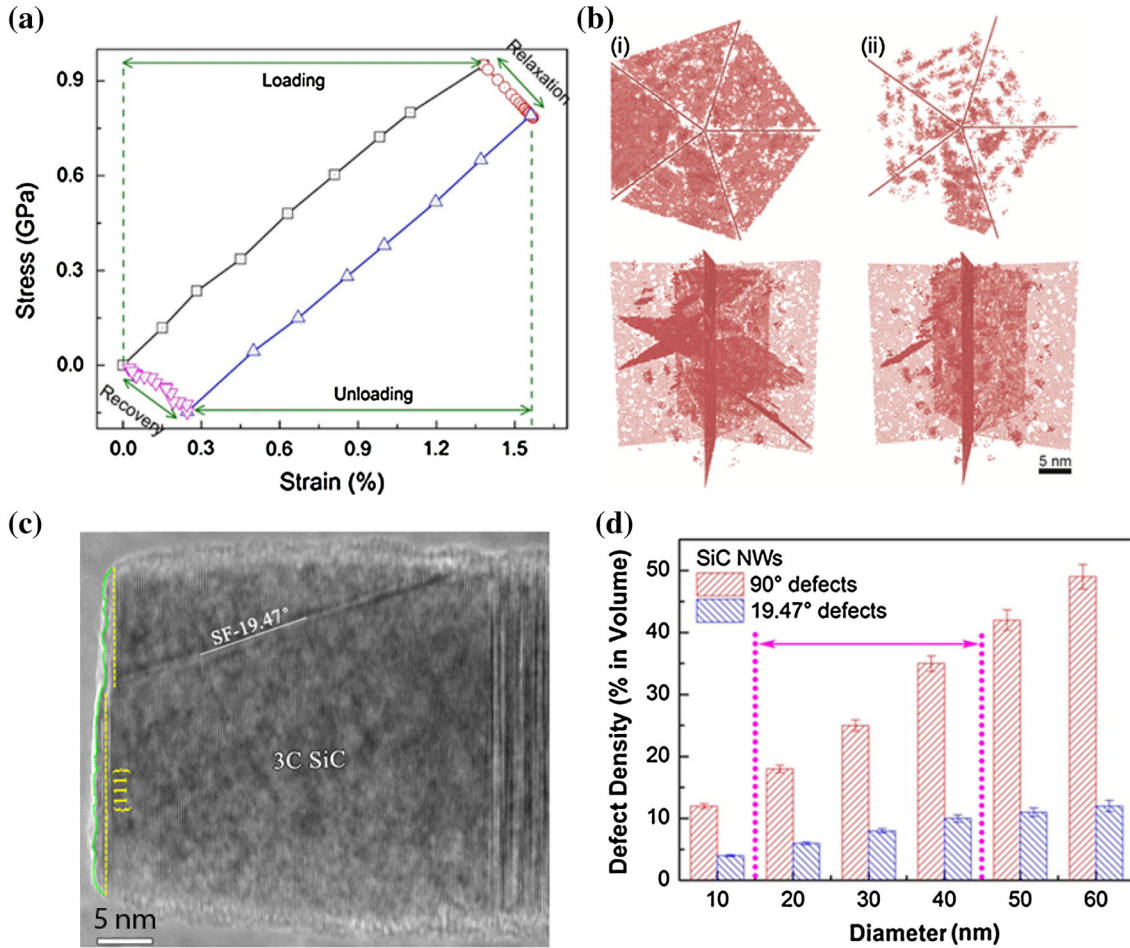
Fig. 5. (a) Measured stress–strain curves for a penta-twinned Ag NW (120 nm in diameter) showing stress relaxation and recoverable plasticity.[78] (b) MD simulations showing fully recoverable plasticity and associated dislocation activities in a 30-nm-diameter penta-twinned Ag nanowire.[78] (i) during relaxation, dislocations are nucleated and confined by the penta-twinned nanostructure; (ii) dislocations retract and disappear during recovery. (c) HRTEM image of the fracture surface of the SiC NW.[113] The loading direction is along the ⟨111⟩ direction. The 19.47° stacking fault is labeled as SF-19.47°. (d) Defect density as a function of NW diameter.[113] Note that the defect density is defined as an average volume percentage of defect parts in a randomly selected segment with a length of 2 μm. The range between the *dotted lines* corresponds to the diameter range tested in this work (17–45 nm). Here, 90° and 19.47° defects refer to highly defective structures and 3C structures with a 19.47° stacking faults, respectively. Images (c) and (d) are reprinted with permission from Ref. 113.

showed that two leading Shockley partial dislocations are usually activated at each dislocation nucleation site on the side surface, which was confirmed by post-mortem TEM images (Fig. 4a and b). Since the intrinsic stacking fault energy is much smaller than the unstable stacking fault energy, slip by the leading partial dislocations is expected to be the dominant deformation mechanism.[78,104] Seo et al. reported a superplastic deformation in single-crystalline Au NWs induced by coherent twin propagation, which converted the initial ⟨110⟩-oriented NW with a rhombic cross-section and {111} side facets to a ⟨100⟩-oriented NW with a rectangular cross-section and {100} side facets (Fig. 4c).[102] Sedlmayr et al. also reported deformation twinning as the dominant deformation process in single-crystalline Au nanowhiskers, but in two different modes: formation of a large number of small twins distributed along the length of the whisker or the

formation of one long twin (Fig. 4d and e).[101] These two deformation modes corresponded to two classes of stress–strain curves, with the former demonstrating continuous flow and the latter showing pronounced stress drops.

Effect of Internal Planar Defects

Penta-twinned NWs contain a fivefold twinned nanostructure with five TBs running along {111} planes in parallel to the longitudinal axis of the NWs and five surface facets along {100} planes with a pentagonal cross-sectional morphology (Fig. 4a). For penta-twinned Ag NWs, a dislocation-mediated, time-dependent and fully reversible plastic behavior was recently reported.[78] Figure 5a shows the stress–strain response during a typical tensile test of a penta-twinned Ag NW in four steps: loading, relaxation, unloading and recovery. During the

relaxation step (i.e., holding the actuator displacement), the stress decreased with time, while the strain increased. After unloading, the strain in the NW completely recovered in about the same amount of time as the relaxation. This behavior originates from the surface nucleation, propagation and retraction of partial dislocations. The TBs and their intrinsic stress field promote retraction of partial dislocations, resulting in full strain recovery. Figure 5b illustrates two snapshots of the MD simulations showing the deformed Ag NW during relaxation and recovery, respectively. Due to the same dislocation/TB interaction, a Bauschinger effect was found for the penta-twinned Ag NWs under cyclic loading.[105] The Bauschinger effect has been reported in thin films and NWs as a result of the heterogeneous distribution of grain size,[106,107] dislocation–grain boundary interaction,[108] surface passivation,[109,110] or twinning–detwinning transition.[111] It should be noted that, for the observed recoverable plasticity, the applied strain to the NWs was relatively small ($<2\%$) and hence the partial dislocations did not transmit across the TBs, which is essential for the recoverable plasticity.[78] When the applied strain was large, the obstructed partial dislocations can transmit across the TBs.

Another effect of the pre-existing TBs in the penta-twinned NWs is pronounced strain hardening.[26,112] Strain hardening was size-dependent: thinner nanowires achieved more hardening and higher ductility. The size-dependent strain hardening was identified as a result of the obstruction of surface-nucleated dislocations by the TBs.[103] This work further revealed the important role of the statistical variation of source strengths of surface-nucleated dislocations in the small-sized nanostructures.[103]

SiC NWs typically consist of three types of microstructures, pure face-centered cubic (3C) structure, 3C structure with an inclined stacking fault ($19.47°$ with respect to the NW length direction), and highly defective structure, in a periodic fashion along the NW length.[113] The SiC NWs were found to deform linear elastically until brittle fracture. The SiC NWs exhibited strong size effect in the fracture strength; that is, the fracture strength increased with decreasing diameter up to over 25 GPa and approaching the theoretical strength of 3C SiC. It is interesting to observe that the cracks initiate and propagate in the 3C segments with the $19.47°$ stacking faults, rather than in the highly defective segments (Fig. 5c). It was observed that the densities of both the 3C structure with an inclined stacking fault ($19.47°$ defect) and highly defective structure ($90°$ defect) decreased with decreasing size (Fig. 5d). Hence, the size effect on fracture strength of SiC NWs was mainly attributed to the size-dependent defect density rather than the surface effect that is common to single-crystalline NWs.[113]

Effect of Point Defects

It is interesting to note the relaxation behavior in penta-twinned AgNWs as described above, which was not observed in single-crystalline Ag nanowhiskers by physical vapor deposition.[78] A high-angle annular dark-field scanning TEM image of the cross-sectional sample showed the presence of vacancy defects near the TBs in the penta-twinned Ag NWs. MD simulations found that vacancy defects reduce dislocation nucleation barrier at the free surface, facilitating stress relaxation.[78] Gianola and co-workers recently reported a strong temperature dependence of strength and its associated scatter in single-crystalline Pd nanowhiskers, suggesting a surface diffusion mechanism as the rate-limiting step needed to promote displacive activity.[38] In both cases, diffusion of point defects plays an essential role in aiding dislocation nucleation from free surfaces, while the exact nature of the diffusion process remains elusive.

Recently, we discovered point defect-induced giant anelasticity in single-crystalline ZnO and *p*-doped Si NWs under bending.[114] At macroscopic scale, anelaticity is usually very small or negligible, especially in single-crystalline materials. Our study found that single-crystalline ZnO and *p*-doped Si NWs can exhibit anelastic behaviour that is up to four orders of magnitude larger than the largest anelasticity observed in bulk materials, with a recovery time scale in the order of minutes. In situ SEM tests of individual NWs showed that, upon removal of the bending load, a substantial portion of the total strain gradually recovers with time following instantaneous recovery of the elastic strain. The observed anelasticity was attributed to stress-gradient-induced migration of point defects.[114]

SUMMARY

A brief review of in situ mechanical characterization of crystalline NWs inside SEM and TEM is presented, including the major experimental methods, selected experimental results and commonly encountered issues. These characterization methods and related nanomechanics studies have contributed tremendously to our understanding of the nanoscale mechanical behaviors. In the past decade, surface effect has received much attention in the community, which certainly plays a critical role in nanomechanical behaviors. On the other hand, single-crystalline NWs, especially the chemically synthesized ones, are known to possess a variety of internal planar defects such as stacking faults and TBs. The interaction between dislocations nucleated from free surfaces and the internal planar defects has led to unusual mechanical behaviors such as recoverable plasticity and strain hardening. Also, a growing body of evidence suggests that a diffusion-controlled process might play an essential role in facilitating nucleation of a first dislocation from free surfaces.

ACKNOWLEDGEMENTS

REFERENCES

1. Y. Xia, P. Yang, Y. Sun, Y. Wu, B. Mayers, B. Gates, Y. Yin, F. Kim, and H. Yan, *Adv. Mater.* 15, 353 (2003).
2. C.M. Lieber and Z.L. Wang, *MRS Bull.* 32, 99 (2007).
3. S. Yao and Y. Zhu, *Adv. Mater.* 27, 1480 (2015).
4. J.R. Greer and J.T.M. De Hosson, *Prog. Mater Sci.* 56, 654 (2011).
5. T. Zhu and J. Li, *Prog. Mater Sci.* 55, 710 (2010).
6. H.S. Park, W. Cai, H.D. Espinosa, and H. Huang, *MRS Bull.* 34, 178 (2009).
7. C.R. Weinberger and W. Cai, *J. Mater. Chem.* 22, 3277 (2012).
8. Y. Zhu, F. Xu, Q.Q. Qin, W.Y. Fung, and W. Lu, *Nano Lett.* 9, 3934 (2009).
9. E.M. Grumstrup, M.M. Gabriel, C.W. Pinion, J.K. Parker, J.F. Cahoon, and J.M. Papanikolas, *Nano Lett.* 14, 6287 (2014).
10. J.K. Diao, K. Gall, and M.L. Dunn, *Nat. Mater.* 2, 656 (2003).
11. L.G. Zhou and H.C. Huang, *Appl. Phys. Lett.* 84, 1940 (2004).
12. H.Y. Liang, M. Upmanyu, and H.C. Huang, *Phys. Rev. B.* 71, 241403 (2005).
13. H.S. Park, K. Gall, and J.A. Zimmerman, *J. Mech. Phys. Solids* 54, 1862 (2006).
14. H. Zheng, A. Cao, C.R. Weinberger, J.Y. Huang, K. Du, J. Wang, Y. Ma, Y. Xia, and S.X. Mao, *Nat. Commun.* 1, 144 (2010).
15. T. Zhu, J. Li, A. Samanta, A. Leach, and K. Gall, *Phys. Rev. Lett.* 100, 25502 (2008).
16. P. Poncharal, Z.L. Wang, D. Ugarte, and W.A. de Heer, *Science* 283, 1513 (1999).
17. M.M.J. Treacy, T.W. Ebbesen, and J.M. Gibson, *Nature* 381, 678 (1996).
18. Q. Qin, F. Xu, Y. Cao, P.I. Ro, and Y. Zhu, *Small* 8, 2571 (2012).
19. C.Q. Chen, Y. Shi, Y.S. Zhang, J. Zhu, and Y.J. Yan, *Phys. Rev. Lett.* 96, 75505 (2006).
20. E.W. Wong, P.E. Sheehan, and C.M. Lieber, *Science* 277, 1971 (1997).
21. B. Wu, A. Heidelberg, and J.J. Boland, *Nat. Mater.* 4, 525 (2005).
22. J.P. Salvetat, G.A.D. Briggs, J.M. Bonard, R.R. Bacsa, A.J. Kulik, T. Stöckli, N.A. Burnham, and L. Forró, *Phys. Rev. Lett.* 82, 944 (1999).
23. Y. Yang, G. Wang, and X. Li, *Nano Lett.* 11, 2845 (2011).
24. M.F. Yu, O. Lourie, M.J. Dyer, K. Moloni, T.F. Kelly, and R.S. Ruoff, *Science* 287, 637 (2000).
25. F. Xu, Q.Q. Qin, A. Mishra, Y. Gu, and Y. Zhu, *Nano Res.* 3, 271 (2010).
26. Y. Zhu, Q. Qin, F. Xu, F. Fan, Y. Ding, T. Zhang, B.J. Wiley, and Z.L. Wang, *Phys. Rev. B* 85, 45443 (2012).
27. M.R. He, Y. Shi, W. Zhou, J.W. Chen, Y.J. Yan, and J. Zhu, *Appl. Phys. Lett.* 95, 091912 (2009).
28. C.H. Lin, H. Ni, X. Wang, M. Chang, Y.J. Chao, J.R. Deka, and X. Li, *Small* 6, 927 (2010).
29. G. Richter, K. Hillerich, D.S. Gianola, R. Monig, O. Kraft, and C.A. Volkert, *Nano Lett.* 9 (2009).
30. Y. Zhu, C. Ke, and H.D. Espinosa, *Exp. Mech.* 47, 7 (2007).
31. M.A. Haque, H.D. Espinosa, and H.J. Lee, *MRS Bull.* 35, 375 (2011).
32. Y. Zhu and T.-H. Chang, *J. Micromech. Microeng.* 25, 093001 (2015).
33. R. Agrawal, B. Peng, and H.D. Espinosa, *Nano Lett.* 9, 4177 (2009).
34. Y. Wang, H.J. Joyce, Q. Gao, X. Liao, H.H. Tan, J. Zou, S.P. Ringer, Z.W. Shan, and C. Jagadish, *Nano Lett.* 11, 1546 (2011).
35. P. Li, Q. Liao, S. Yang, X. Bai, Y. Huang, X. Yan, Z. Zhang, S. Liu, P. Lin, Z. Kang, and Y. Zhang, *Nano Lett.* 14, 480 (2014).
36. Y. Yue, P. Liu, Z. Zhang, X. Han, and E. Ma, *Nano Lett.* 11, 3151 (2011).
37. J. Wang, Z. Zeng, C.R. Weinberger, Z. Zhang, T. Zhu, and S.X. Mao, *Nat. Mater.* 14, 594 (2015).
38. L.Y. Chen, M.-R. He, J. Shin, G. Richter, and D.S. Gianola, *Nat. Mater.* 14, 707 (2015).
39. H.D. Espinosa, R.A. Bernal, and T. Filleter, *Small* 8, 3233 (2012).
40. R. Ramachandramoorthy, R. Bernal, and H.D. Espinosa, *ACS Nano* 9, 4675 (2015).
41. D.M. Tang, C.L. Ren, M.S. Wang, X. Wei, N. Kawamoto, C. Liu, Y. Bando, M. Mitome, N. Fukata, and D. Golberg, *Nano Lett.* 12, 1898 (2012).
42. W. Ding, L. Calabri, X. Chen, K.M. Kohlhaas, and R.S. Ruoff, *Compos. Sci. Technol.* 66, 1112 (2006).
43. M.-F. Yu, G.J. Wagner, R.S. Ruoff, and M.J. Dyer, *Phys. Rev. B* 66, 073406 (2002).
44. C.Q. Sun, *Prog. Solid State Chem.* 35, 1 (2007).
45. S. Hoffmann, F. Östlund, J. Michler, H.J. Fan, M. Zacharias, S.H. Christiansen, and C. Ballif, *Nano Lett.* 6, 622 (2006).
46. C.Q. Chen and J. Zhu, *Appl. Phys. Lett.* 90 (2007).
47. D.S. Gianola and C. Eberl, *JOM* 61, 24 (2009).
48. D. Kiener and A.M. Minor, *Nano Lett.* 11, 3816 (2011).
49. Q. Yu, L. Qi, K. Chen, R.K. Mishra, J. Li, and A.M. Minor, *Nano Lett.* 12, 887 (2012).
50. D. Kiener, W. Grosinger, G. Dehm, and R. Pippan, *Acta Mater.* 56, 580 (2008).
51. C. Eberl, D.S. Gianola, and R. Thompson, *File No. 12413* (Natick, MA: The Mathworks, Inc., 2006).
52. X. Han, K. Zheng, Y.F. Zhang, X. Zhang, Z. Zhang, and Z.L. Wang, *Adv. Mater.* 19, 2112 (2007).
53. S. Orso, U.G.K. Wegst, C. Eberl, and E. Arzt, *Adv. Mater.* 18, 874 (2006).
54. M.A. Haque and M.T.A. Saif, *Exp. Mech.* 42, 123 (2002).
55. M.A. Haque and M.T.A. Saif, *Proc. Natl. Acad. Sci. USA* 101, 6335 (2004).
56. K.J. Hemker and W.N. Sharpe, *Ann. Rev. Mater. Res.* 37, 93 (2007).
57. Y. Zhu and H.D. Espinosa, *Proc. Natl. Acad. Sci. USA* 102, 14503 (2005).
58. Y. Zhu, N. Moldovan, and H.D. Espinosa, *Appl. Phys. Lett.* 86, 13506 (2005).
59. Y. Zhu, A. Corigliano, and H.D. Espinosa, *J. Micromech. Microeng.* 16, 242 (2006).
60. H.D. Espinosa, Y. Zhu, and N. Moldovan, *J. Microelectromech. Syst.* 16, 1219 (2007).
61. D.F. Zhang, W. Drissen, J.M. Breguet, R. Clavel, and J. Michler, *J. Micromech. Microeng.* 19 (2009).
62. B. Pant, B.L. Allen, T. Zhu, K. Gall, and O.N. Pierron, *Appl. Phys. Lett.* 98, 053506 (2011).
63. L.Y. Chen, S. Terrab, K.F. Murphy, J.P. Sullivan, X. Chen, and D.S. Gianola, *Rev. Sci. Instrum.* 85, 013901 (2014).
64. T.H. Chang and Y. Zhu, *Appl. Phys. Lett.* 103, 263114 (2013).
65. Z.W. Shan, R.K. Mishra, S.A. Syed Asif, O.L. Warren, and A.M. Minor, *Nat. Mater.* 7, 115 (2008).
66. A.T. Jennings, M.J. Burek, and J.R. Greer, *Phys. Rev. Lett.* 104, 135503 (2010).
67. M.D. Uchic, P.A. Shade, and D.M. Dimiduk, *Annu. Rev. Mater. Res.* 39, 361 (2009).
68. C.L. Hsin, W. Mai, Y. Gu, Y. Gao, C.T. Huang, Y. Liu, L.-J. Chen, and Z.L. Wang, *Adv. Mater.* 20, 3919 (2008).
69. K.F. Murphy, L.Y. Chen, and D.S. Gianola, *Nanotechnology* 24, 235704 (2013).
70. Q. Qin and Y. Zhu, *Appl. Phys. Lett.* 102, 013101 (2013).
71. A. Soudi, E.H. Khan, J.T. Dickinson, and Y. Gu, *Nano Lett.* 9, 1844 (2009).
72. J.E. Allen, E.R. Hemesath, D.E. Perea, J.L. Lensch-Falk, Z.Y. Li, F. Yin, M.H. Gass, P. Wang, A.L. Bleloch, R.E. Palme, and L.J. Lauhon, *Nat. Nanotechnol.* 3, 168 (2008).

73. F.J. Lopez, E.R. Hemesath, and L.J. Lauhon, *Nano Lett.* 9, 2774 (2009).
74. Y. Sun and Y. Xia, *Adv. Mater.* 14, 833 (2002).
75. K.K. Caswell, C.M. Bender, and C.J. Murphy, *Nano Lett.* 3, 667 (2003).
76. J. Sun, L. He, Y.C. Lo, T. Xu, H. Bi, L. Sun, Z. Zhang, S.X. Mao, and J. Li, *Nat. Mater.* 13, 1007 (2014).
77. C.A. Schuh, J.K. Mason, and A.C. Lund, *Nat. Mater.* 4, 617 (2005).
78. Q. Qin, S. Yin, G. Cheng, X. Li, T.-H. Chang, G. Richter, Y. Zhu, and H. Gao, *Nat. Commun.* 6, 5983 (2015).
79. J. Li, *Nat. Mater.* 14, 656 (2015).
80. J. He and C.M. Lilley, *Nano Lett.* 8, 1798 (2008).
81. G.Y. Jing, H.L. Duan, X.M. Sun, Z.S. Zhang, J. Xu, Y.D. Li, J.X. Wang, and D.P. Yu, *Phys. Rev. B* 73, 235409 (2006).
82. F. Song, G.L. Huang, H.S. Park, and X.N. Liu, *Int. J. Solids Struct.* 48, 2154 (2011).
83. R.E. Miller and V.B. Shenoy, *Nanotechnology* 11, 139 (2000).
84. H.W. Shim, L.G. Zhou, H. Huang, and T.S. Cale, *Appl. Phys. Lett.* 86, 151912 (2005).
85. R. Agrawal, B. Peng, E. Gdoutos, and H.D. Espinosa, *Nano Lett.* 8, 3668 (2008).
86. A. Heidelberg, L.T. Ngo, B. Wu, M.A. Phillips, S. Sharma, T.I. Kamins, J.E. Sader, and J.J. Boland, *Nano Lett.* 6, 1101 (2006).
87. M. Tabib-Azar, M. Nassirou, R. Wang, S. Sharma, T.I. Kamins, M.S. Islam, and R.S. Williams, *Appl. Phys. Lett.* 87, 113102 (2005).
88. M.J. Gordon, T. Baron, F. Dhalluin, P. Gentile, and P. Ferret, *Nano Lett.* 9, 525 (2009).
89. B. Lee and R.E. Rudd, *Phys. Rev. B* 75, 195328 (2007).
90. K. Kang and W. Cai, *Philos. Mag.* 87, 2169 (2007).
91. X.X. Li, T. Ono, Y.L. Wang, and M. Esashi, *Appl. Phys. Lett.* 83, 3081 (2003).
92. A.V. Desai and M.A. Haque, *Sensors Actuators A Phys.* 134, 169 (2007).
93. X.D. Bai, P.X. Gao, Z.L. Wang, and E.G. Wang, *Appl. Phys. Lett.* 82, 4806 (2003).
94. B. Wen, J.E. Sader, and J.J. Boland, *Phys. Rev. Lett.* 101, 175502 (2008).
95. H.S. Park, *J. Appl. Phys.* 103, 123504 (2008).
96. L. Chen, G. Richter, J. Sullivan, and D. Gianola, *Phys. Rev. Lett.* 109, 125503 (2012).
97. M.T. McDowell, A.M. Leach, and K. Gall, *Nano Lett.* 8, 3613 (2008).
98. Z. Wu, Y.-W. Zhang, M.H. Jhon, H. Gao, and D.J. Srolovitz, *Nano Lett.* 12, 910 (2012).
99. C. Peng, Y. Zhan, and J. Lou, *Small* 8, 1889 (2012).
100. W. Liang, M. Zhou, and F. Ke, *Nano Lett.* 5, 2039 (2005).
101. A. Sedlmayr, E. Bitzek, D.S. Gianola, G. Richter, R. Mönig, and O. Kraft, *Acta Mater.* 60, 3985 (2012).
102. J.H. Seo, Y. Yoo, N.Y. Park, S.W. Yoon, H. Lee, S. Han, S.-W. Lee, T.Y. Seong, S.C. Lee, K.B. Lee, P.R. Cha, H.S. Park, B. Kim, and J.P. Ahn, *Nano Lett.* 11, 3499 (2011).
103. S. Narayanan, G. Cheng, Z. Zeng, Y. Zhu, and T. Zhu, *Nano Lett.* 15, 4037 (2015).
104. H. Van Swygenhoven, P.M. Derlet, and A.G. Froseth, *Nat. Mater.* 3, 399 (2004).
105. R.A. Bernal, A. Aghaei, S. Lee, S. Ryu, K. Sohn, J. Huang, W. Cai, and H.D. Espinosa, *Nano Lett.* 15, 139 (2015).
106. J. Rajagopalan, J.H. Han, and M.T.A. Saif, *Science* 315, 1831 (2007).
107. J. Rajagopalan, C. Rentenberger, H. Peter Karnthaler, G. Dehm, and M.T.A. Saif, *Acta Mater.* 58, 4772 (2010).
108. F. Mompiou, D. Caillard, M. Legros, and H. Mughrabi, *Acta Mater.* 60, 3402 (2012).
109. Y. Xiang and J.J. Vlassak, *Scripta Mater.* 53, 177 (2005).
110. A.T. Jennings, C. Gross, F. Greer, Z.H. Aitken, S.W. Lee, C.R. Weinberger, and J.R. Greer, *Acta Mater.* 60, 3444 (2012).
111. S. Lee, J. Im, Y. Yoo, E. Bitzek, D. Kiener, G. Richter, B. Kim, and S.H. Oh, *Nat. Commun.* 5, 3033 (2014).
112. T. Filleter, S. Ryu, K. Kang, J. Yin, R.A. Bernal, K. Sohn, S. Li, J. Huang, W. Cai, and H.D. Espinosa, *Small* 8, 2986 (2012).
113. G. Cheng, T.-H. Chang, Q. Qin, H. Huang, and Y. Zhu, *Nano Lett.* 14, 754 (2014).
114. G. Cheng, C. Miao, Q. Qin, J. Li, F. Xu, H. Haftbaradaran, E.C. Dickey, H. Gao, and Y. Zhu, *Nat. Nanotechnol.* 10, 687 (2015).